

Uncertainty in the ENSO amplitude change from the past to the future

Masahiro Watanabe¹, Jong-Seong Kug², Fei-Fei Jin³, Mat Collins⁴,

Masamichi Ohba⁵, and Andrew T. Wittenberg⁶

1 Atmosphere and Ocean Research Institute, the University of Tokyo, Japan

2 Korea Ocean Research and Development Institute, Korea

3 Department of Meteorology, University of Hawaii at Manoa, USA

4 College of Engineering Mathematics and Physical Sciences, University of Exeter,
and Met Office Hadley Centre, UK

5 Central Research Institute of Electric Power Industry, Japan

6 NOAA Geophysical Fluid Dynamics Laboratory, USA

Geophysical Research Letters

Submitted on July 26, 2012

Revised on September 5, 2012

Corresponding author:

M. Watanabe,

Atmosphere and Ocean Research Institute, University of Tokyo,

Kashiwa, Chiba 277-8568, Japan

(e-mail: hiro@ori.u-tokyo.ac.jp)

1 **Abstract.** Due to errors in complex coupled feedbacks that compensate differently in
2 different global climate models, as well as nonlinear nature of El Niño-Southern Oscillation
3 (ENSO), there remain difficulties in detecting and evaluating the reason for the past and
4 future changes in the ENSO amplitude, $\sigma_{\text{niño}}$. Here we use physics parameter ensembles, in
5 which error compensation was eliminated by perturbing model parameters, to explore
6 relationships between mean climate and variability. With four such ensembles we find a
7 strong relationship between $\sigma_{\text{niño}}$ and the mean precipitation over the eastern equatorial
8 Pacific ($\bar{P}_{\text{niño}}$). This involves a two-way interaction, in which the wetter mean state with
9 greater $\bar{P}_{\text{niño}}$ acts to increase the ENSO amplitude by strengthening positive coupled
10 feedbacks. Such a relationship is also identified in 11 single-model historical climate
11 simulations in the Coupled Model Intercomparison Project phase 5 despite mean precipitation
12 biases apparently masking the relationship in the multi-model ensemble (MME). Taking
13 changes in $\sigma_{\text{niño}}$ and $\bar{P}_{\text{niño}}$ between pre-industrial and recent periods eliminates the bias, and
14 therefore results in a robust $\sigma_{\text{niño}} - \bar{P}_{\text{niño}}$ connection in MME, which suggests a 10-15%
15 increase in the ENSO amplitude since pre-industrial era mainly due to changing mean state.
16 However, the $\sigma_{\text{niño}} - \bar{P}_{\text{niño}}$ connection is less clear for their future changes, which are still
17 greatly uncertain.

18

19 **1. Introduction**

20 With the continuous development of general circulation models (GCMs) over the last
21 few decades, the simulation of ENSO under present climate conditions has become more
22 realistic than before in terms of frequency and spatial structure [*AchutaRao and Sperber*

23 2006]. Further, accumulation of recent studies has advanced our understanding a number of
24 processes involved in the dynamics of ENSO [Collins et al. 2010]. Nevertheless, a
25 fundamental ENSO property, namely, amplitude, is still highly model-dependent because of
26 competing feedback processes in different GCMs [Meehl et al. 2007a, Guilyardi et al. 2009a,
27 Vecchi and Wittenberg 2010]. In any member of a multi-model ensemble (MME), there is a
28 potential for compensating errors and structural differences, i.e., differences in
29 parameterization scheme, dynamical core, and resolution, making it difficult to understand the
30 diversity in the ENSO amplitude across the models using a simple metric. It might be,
31 however, possible to attribute changing ENSO amplitude to specific processes in
32 structurally-similar model ensembles in which error compensation may be eliminated by
33 perturbing model parameters.

34 Recent studies indicate that among the various causes of error and uncertainty in ENSO
35 simulations in GCM ensembles, the atmospheric model serves as an important source of
36 diversity in GCM ensembles [Guilyardi et al. 2004, Philip et al. 2010]. In particular,
37 parameterization schemes for cumulus convection, which affect both positive Bjerknes and
38 negative heat flux feedbacks, greatly influence the ENSO properties [Neale et al. 2008,
39 Guilyardi et al. 2009b, Watanabe et al. 2011, Kim et al. 2011]. Here we use four sets of GCM
40 ensembles in which the atmospheric model parameters have been perturbed (see the next
41 section). The two base models of our perturbed parameter ensembles (PPE) were included in
42 the Coupled Model Intercomparison Project phase 3 (CMIP3) and show great ability to
43 reproduce the present tropical climate [van Oldenborgh et al. 2005, Meehl et al. 2007b]; the
44 other two were developed after CMIP3 and are included in a more recent ensemble of CMIP5

45 [Taylor et al. 2012], which is partly available as of this writing. In addition to the
46 century-long control experiments using pre-industrial external conditions, we performed
47 experiments involving either abrupt doubling or a 1% increase in the atmospheric CO₂
48 concentration for each model and parameter set in order to evaluate changes in the ENSO
49 amplitude by global warming. With these experiments, we found that the ENSO amplitude is
50 well measured by the mean rainfall over the eastern equatorial Pacific. This relationship is
51 then applied to CMIP MMEs to discuss the robustness. The evaluation of CMIP5 models is
52 ongoing in parallel with this study, but preliminary results reveal that the diversity of the
53 simulated ENSO property is still large despite the reduced amplitude error over the historical
54 runs in CMIP5 compared to CMIP3 [Guilyardi et al. 2012]. This may not be surprising given
55 the error compensation in MME, but our results suggest that there is a common signal of the
56 ENSO intensification from the pre-industrial era to present, which can be interpreted in terms
57 of the mean state change.

58

59 **2. Model ensembles**

60 We used the following perturbed parameter ensembles. An ensemble based on the third
61 version of the Hadley Centre climate model (HadCM3) had 17 members, in which 33
62 atmospheric model parameters were perturbed [Toniazzi et al. 2008]. In each model, a set of
63 pre-industrial control and 1% CO₂ increasing runs was performed for 150 years. The other
64 three models, the fifth version of the Model for Interdisciplinary Research on Climate
65 (MIROC5) [Watanabe et al. 2011], the Geophysical Fluid Dynamics Laboratory coupled
66 model version 2.1 (GFDL CM2.1) [Kim et al. 2011], and the fourth version of the Community

67 Climate System Model (CCSM4) [Gent et al. 2011], each employ a single-parameter
68 ensemble, in which one parameter controlling the cumulus entrainment process is varied
69 among the 4, 5, and 7 members, respectively. Besides control simulations for 100 years using
70 these models, doubled CO₂ experiments were carried out for the same periods.

71 It is cautioned that different types of the ensembles, i.e. multi-model and parameter
72 ensembles, should not be treated equally because they represent different kinds of uncertainty.
73 Therefore, we did not merge the parameter ensembles with the CMIP MMEs. The combined
74 multi-model statistics are generated by prescribing the sample size for each model as $N = 4$
75 and repeating the calculation 500 times with randomly selected samples from three models
76 with larger samples. All the model fields have been re-gridded to a regular $2.5^\circ \times 2.5^\circ$ grid
77 before the analysis. The ENSO amplitude ($\sigma_{\text{niño}}$) is defined by the std dev of monthly, linearly
78 de-trended Niño 3 SST anomalies for each period. Since the de-trending is crucial for
79 evaluating $\sigma_{\text{niño}}$ especially in the CMIP MMEs and the HadCM3 parameter ensemble, we
80 have also tested a 1-20 year bandpass filter when calculating $\sigma_{\text{niño}}$, which did not change the
81 conclusions.

82 We also use CMIP3 and CMIP5 MMEs, consisting of 24 and 18 models, respectively
83 (see Meehl et al. 2007b for CMIP3 models and Supplementary Table S1 for CMIP5 models
84 and experiments). Monthly mean SST and precipitation fields for 1940-1999 are obtained
85 from the 20th century simulations of CMIP3 and CMIP5, and also those fields for 2040-2099
86 from the Representative Concentration Pathway (RCP) 4.5 scenario experiments and for the
87 entire period from the pre-industrial control experiments of CMIP5.

88

89 3. Results

90 The relevance of parameter ensembles may depend on the ability of the base models in
91 simulating ENSO. When the typical anomalies in sea surface temperature (SST), precipitation
92 (P), and surface wind stresses during El Niño obtained from the CMIP3 MME and our
93 parameter ensemble are compared with observations, both ensembles reproduce the observed
94 features of El Niño (see Supplementary Fig. S1). The root-mean-square errors of the
95 ENSO-related P and zonal stress (τ_x) anomalies indicate that our ensemble can simulate El
96 Niño and the associated atmospheric response at least as realistically as the CMIP3 MME.

97 It is likely that the ENSO characteristics are controlled to some extent by the mean
98 atmosphere-ocean state in the tropical Pacific [e.g. *An et al. 2008*]. To elucidate the details of
99 the ENSO amplitude change across the members, we examine the relationship between the
100 ENSO amplitude as measured by $\sigma_{\text{niño}}$ and the annual-mean precipitation climatology (\bar{P}) in
101 the control integrations of our parameter ensembles. By equally weighting the four models, a
102 multi-model mean property of the correlation between $\sigma_{\text{niño}}$ and \bar{P} is obtained (Fig. 1a). A
103 significant positive correlation is found over the central-eastern equatorial Pacific where \bar{P}
104 is less than 2.5 mm dy^{-1} , surrounded by a negative correlation over the western Pacific and the
105 off-equatorial regions. This implies that the ENSO tends to be stronger in models having a
106 wetter mean condition over the equatorial cold tongue. The above relationship is identified in
107 each parameter ensemble but not in CMIP3 and CMIP5 MMEs (Fig. S2).

108 The scatter diagram between $\sigma_{\text{niño}}$ and \bar{P} over the Niño 3 region ($\bar{P}_{\text{niño}}$) for each model
109 provides further details (Fig. 1b–e). In the pre-industrial control experiments (blue symbols),
110 $\bar{P}_{\text{niño}}$ is $1\text{--}2 \text{ mm dy}^{-1}$, which includes the observation (‘×’ mark), with $\sigma_{\text{niño}}$ varying from 0.3

111 to 1.5 K. All the ensembles exhibit a positive correlation between $\sigma_{\text{niño}}$ and $\bar{P}_{\text{niño}}$, whereas the
112 mean values and the regression slope are different from each other. The worst linear fitting in
113 HadCM3 may be attributed to the multiple parameters being systematically perturbed and the
114 use of flux-adjustments to prevent model drifts [Toniazzi *et al.* 2008]. The $\sigma_{\text{niño}}-\bar{P}_{\text{niño}}$
115 relationship in the doubled CO₂ and 1% increased CO₂ experiments (red symbols) is
116 discussed later.

117 In two of the four models (MIROC5 and GFDL CM2.1), the mechanisms of ENSO
118 intensification with increased $\bar{P}_{\text{niño}}$ in the control runs have been clarified [Watanabe *et al.*
119 2011, Kim *et al.* 2011, see also Fig. S3]. When the mean atmosphere becomes wet over the
120 cold tongue, it allows an ENSO-induced precipitation anomaly to occur there, causing the τ_x
121 response to the ENSO-related SST anomaly to shift eastward. The zonal shift in τ_x results in a
122 stronger response in the eastern Pacific thermocline and a larger covariance between the
123 anomalous zonal current and SST, which strengthens the El Niño growth [Kang and Kug
124 2002]. These processes, corresponding to enhanced thermocline and zonal advective
125 feedbacks [Collins *et al.* 2010], together with a stronger atmospheric noise forcing, boost
126 ENSO amplitude in a wetter atmospheric mean state [Kug *et al.* 2008]. Therefore, $\bar{P}_{\text{niño}}$
127 provides an indicator of the efficacy of several feedback processes associated with the wind
128 stress anomalies.

129 It is often argued that the ENSO cycle interacts with the mean state in the tropical Pacific
130 [Guilyardi *et al.* 2006, Choi *et al.* 2009]. This suggests an alternative possibility in the
131 interpretation of the $\sigma_{\text{niño}}-\bar{P}_{\text{niño}}$ relationship identified in Fig. 1; stronger ENSO in a model
132 works to increase $\bar{P}_{\text{niño}}$ due to an asymmetry in the precipitation response to the ENSO phase

133 (i.e., P can increase to warmer SST but cannot decrease much to colder SST). This possibility
 134 can be examined by using the so-called probability density function (PDF) method for
 135 reconstructing \bar{P} [Watanabe and Wittenberg 2012].

$$136 \quad \bar{P}_{\text{niño}} = \int f(T)C(T)dT, \quad (1)$$

137 where T is the Niño 3 SST, $f(T)$ is the PDF of T , and $C(T)$ is the composite of the Niño 3 P
 138 with respect to T (see inset in Fig. 2). Suppose (1) applied to the respective parameter
 139 ensemble, the mean precipitation can be expressed with four terms by dividing each quantity
 140 into a reference value $(\)_0$ and the deviation from the reference $(\)'$.

$$141 \quad \begin{aligned} \bar{P}_{\text{niño}} - \bar{P}_0 &= \int f'C_0(T)dT + \int f_0C'(T)dT + \int fC'(T)dT \\ &= \int (f - \hat{f})C_0(T)dT + \int (\hat{f} - f_0)C_0(T)dT + \int f_0C'(T)dT + \int fC'(T)dT, \end{aligned} \quad (2)$$

142 where the lhs of (2) indicates the mean precipitation excess in each member. $C_0(T)$ is
 143 simply obtained from the ensemble average, while f_0 is calculated by averaging f after the
 144 mean position is shifted to each other so that it ensures a plausible mean shape. Since f'
 145 consists not only of the difference in the ENSO property but of the difference in mean SST, it
 146 is further divided by introducing a virtual PDF, \hat{f} , which has the same shape as f_0 except
 147 that the mean position follows f . The first term on the rhs of the second equation represents
 148 the varying PDF width due to the ENSO amplitude change, and is referred to as the ENSO
 149 amplitude feedback. The second term is the effect of mean SST change, while the third term
 150 represents the different sensitivity of P to the underlying SST. The last term accounts for
 151 nonlinearity between f and $C(T)$, which is much smaller than the other terms. The ENSO
 152 feedback to the mean state may also occur via an asymmetry between El Niño and La Niña

153 [An and Jin 2004], acting to increase the mean SST, which is implicitly included in the
154 second term.

155 When we apply the PDF method to each of the four parameter ensembles, the
156 reconstruction of (1) works by definition in reproducing $\bar{P}_{\text{niño}}$ (Fig. 2). The relative
157 contribution of four terms in (2) to the diversity in $\bar{P}_{\text{niño}}$ can be quantified by calculating the
158 linear regression coefficient of each term against the reconstructed mean precipitation.
159 Plotting these values for each parameter ensemble indicates that the diversity in $\bar{P}_{\text{niño}}$ among
160 different members arises from all the terms except for nonlinearity (Fig. 2). The differences in
161 the sensitivity of precipitation to SST dominate in HadCM3 and CCSM4, whereas the mean
162 SST effect greatly works to increase $\bar{P}_{\text{niño}}$ in MIROC5 and GFDL CM2.1. The ENSO
163 amplitude feedback to the mean rainfall is positive in all the models and is not negligible; it
164 accounts for about 40 % on average. Thus, the $\sigma_{\text{niño}}-\bar{P}_{\text{niño}}$ relationship identified in the
165 parameter ensembles involves a two-way coupling between ENSO and the mean state, in
166 which the mean state control of ENSO is slightly greater than the ENSO rectification to the
167 mean state.

168 Unlike our combined parameter ensemble, the CMIP MMEs show neither a significant
169 correlation between $\sigma_{\text{niño}}$ and \bar{P} (Fig. S2) nor a systematic tendency for a future ENSO
170 amplitude change. The scatter diagram of $\sigma_{\text{niño}}$ against $\bar{P}_{\text{niño}}$ for the latter half of the 20th
171 century, 1940–1999, obtained from the historical experiments, appears to be very different
172 from our parameter ensemble (Fig. 3a). For the recent 60 years, $\bar{P}_{\text{niño}}$ contains large errors
173 compared with Fig. 1b–e, and the ENSO amplitude is even negatively correlated with $\bar{P}_{\text{niño}}$
174 in the ensemble, which remains the same in the 21st century (figure not shown).

175 In addition to a large bias in $\bar{P}_{\text{niño}}$ in the CMIP ensembles, error compensation occurring
 176 differently in different models may mask the subtle dependence of $\sigma_{\text{niño}}$ on $\bar{P}_{\text{niño}}$. However,
 177 we may still see the relationship akin to Fig. 1b-e in MME if it were not the single-member
 178 ensemble. Fortunately, ensembles of the historical runs, in which different initial conditions
 179 have been adopted, are available for some of the CMIP5 models. The plot of $\sigma_{\text{niño}}$ and $\bar{P}_{\text{niño}}$
 180 for the above ensemble indeed shows that 11 among 12 models reveal a positive relationship
 181 within the respective model (Fig. 3b). While the ensemble size and the spread across members
 182 are small, the commonly found positive correlation, 0.84 on average, supports robustness of
 183 the $\sigma_{\text{niño}}-\bar{P}_{\text{niño}}$ relationship. In the absence of changes in model parameters or the external
 184 radiative forcing, the ENSO amplitude feedback dominates the other terms in (2) (Fig. S4).

185 The above results not only provide a useful metric that measures the simulated ENSO
 186 amplitude but also can be used to explain historical changes in the ENSO intensity. To reduce
 187 the sampling noise due to internal variability, we take differences between 1940-1999 and an
 188 entire period of the pre-industrial experiment performed with the 1850 external forcing in
 189 each model. The change in \bar{P} from the pre-industrial to recent periods, denoted as $\Delta\bar{P}$, is
 190 characterized by increase in the tropics and high latitudes while decrease in the subtropics
 191 (Fig. S5a). The value of $\Delta\bar{P}_{\text{niño}}$ is different among models, but is clearly related with the
 192 change in $\sigma_{\text{niño}}$, $\Delta\sigma_{\text{niño}}$ (Fig. 4a). While $\Delta\sigma_{\text{niño}}$ appears insensitive to $\Delta\bar{P}_{\text{niño}}$ in a few models
 193 (INM-CM4, MRI-CGCM3, and NorESM1-M) that show slight decrease in precipitation, the
 194 overall relationship in MME is linear with the correlation coefficient of 0.91. The relative
 195 contribution of the ENSO-mean state feedbacks examined following (2) was different from
 196 Figs. 2 and S4, i.e., the weak ENSO amplitude feedback except for limited models showing

197 strong ENSO. The increase in mean SST works to increase $\bar{P}_{\text{niño}}$, which is partly cancelled by
198 the changing precipitation sensitivity (Fig. S6). This dominant effect of the mean SST
199 increase for $\Delta\bar{P}_{\text{niño}}$ is also seen in the increased CO₂ experiments of our parameter ensembles.
200 While the magnitude and pattern of $\Delta\bar{P}$ cannot be verified due to lack of the long-term
201 precipitation measurements [Xie and Arkin 1997], there are observed SST data for more than
202 a century [Rayner et al. 2003, Kaplan et al. 1998], which indicate an increase of $\sigma_{\text{niño}}$ by
203 10-15 % between 1871-1930 and 1940-1999 periods [Kang et al. 2006, also Fig. 4a]. With the
204 limited SST measurements before the World War II, which were used to re-construct the
205 global map, $\sigma_{\text{niño}}$ for 1871-1930 is less reliable than that for 1940-1999. Yet, the strong
206 $\Delta\sigma_{\text{niño}}-\Delta\bar{P}_{\text{niño}}$ relationship in the CMIP5 MME, which also gives the ensemble-mean estimate
207 of $\Delta\sigma_{\text{niño}}$ within the observational estimates, supports that the increased ENSO variance since
208 the pre-industrial era is physically relevant. However, the natural amplitude modulation of the
209 ENSO activity is considerably large [Wittenberg 2009], implying that the signal-to-noise ratio
210 for the past $\Delta\sigma_{\text{niño}}$ should be carefully evaluated.

211

212 **4. Discussion on future changes in ENSO amplitude**

213 Given that future changes in the ENSO amplitude are not yet conclusive with CMIP3
214 MME [Meehl et al. 2007a], a question of whether the $\sigma_{\text{niño}}-\bar{P}_{\text{niño}}$ relationship can be used to
215 explain the diversity in the changes in future ENSO amplitude is of great concern. Some
216 common signals of climate change in the tropical Pacific mean state in global warming
217 experiments, such as the weakening of the Walker circulation [Vecchi et al. 2006] and an
218 increase in the equatorial Pacific SST [Meehl et al. 2007a], apparently act to increase $\bar{P}_{\text{niño}}$. In

219 the doubled CO₂ and 1% increased CO₂ experiments of our parameter ensembles, $\bar{P}_{\text{niño}}$ was
220 shifted toward larger values with little change in the slope of $\partial\sigma_{\text{niño}}/\partial\bar{P}_{\text{niño}}$ (Fig. 1b-e). In
221 addition to all but one of the ensemble-mean values showing positive changes in $\sigma_{\text{niño}}$ as well,
222 most of the individual realizations—all members in MIROC5 and HadCM3, 4 among 5 in
223 GFDL CM2.1, and 3 among 7 in CCSM4— show the same tendency. In HadCM3, a
224 systematic positive shift is also observed in $\bar{P}_{\text{niño}}$, which probably arises from transient
225 simulation that tends to amplify the precipitation response. These results suggest an
226 amplification of ENSO in a warmed climate, consistent with some of the GCM studies [*Yeh et*
227 *al. 2006, Cherchi et al. 2008, Park et al. 2009*]. However, this idea is not strongly supported
228 by the future scenario experiments in CMIP5 despite a common change of the positive $\Delta\bar{P}_{\text{niño}}$
229 between 1940-1999 and 2040-2099 (Fig. 4b). This may not be surprising given coupled
230 feedback processes acting differently to the El Niño growth in a changing climate [*Collins et*
231 *al. 2010*], but the similarity in the past and future $\Delta\bar{P}$ patterns is somewhat puzzling (Fig.
232 S5b). One possibility is that, in a warmed climate, there is another model-dependent
233 suppression mechanism for ENSO, which emerges more slowly than the positive coupled
234 feedback represented by the $\sigma_{\text{niño}}-\bar{P}_{\text{niño}}$ relationship. A deeper analysis for the mechanism of
235 the ENSO amplitude control in CMIP5 experiments is expected to unravel why the ENSO
236 amplitude change in a warmer climate is so uncertain.

237

238 **Acknowledgements** We thank E. Guilyardi, S. Power, J. N. Brown, and an anonymous
239 reviewer for useful comments. We also acknowledge M. Arai, N. Hirota and Y.-S. Jang for
240 the data processing. This work was supported by the Innovative Program of Climate Change

241 Projection for the 21st Century from MEXT, Japan, the Mitsui Environment Fund C-042, NSF
242 ATM 1034439, NOAA NA10OAR4310200, and DOE DESC0005110.

243

244 **References**

245 AchutaRao, K., and K. Sperber (2006), ENSO simulations in coupled ocean-atmosphere
246 models: Are the current models better? *Clim. Dyn.*, **27**, 1-15.

247 An, S.-I., and F.-F. Jin (2004) Nonlinearity and asymmetry of ENSO. *J. Climate*, **17**,
248 2399-2412.

249 An, S.-I., J.-S. Kug, Y.-G. Ham, and I. S. Kang (2008), Successive modulation of ENSO to
250 the future greenhouse warming. *J. Climate*, **21**, 3-21.

251 Cherchi, A., S. Masina, and A. Navarra (2008), Impact of extreme CO₂ levels on tropical
252 climate: A CGCM study. *Clim. Dyn.*, **31**, 743-758.

253 Choi, J., S.-I. An, B. Dewitte, and W. M. Hsieh (2009), Interactive feedback between the
254 tropical Pacific decadal oscillation and ENSO in a coupled general circulation model. *J.*
255 *Climate*, **22**, 6597-6611.

256 Collins, M., and Coauthors (2010), The impact of global warming on the tropical Pacific
257 Ocean and El Niño. *Nature Geo.*, **3**, 391-397.

258 Gent, P. R., and Coauthors (2011), The community climate system model version 4. *J.*
259 *Climate*, **24**, 4973-4991.

260 Guilyardi, E., and Coauthors (2004), Representing El Niño in coupled ocean-atmosphere
261 GCMs: The role of the atmospheric component. *J. Climate*, **17**, 4623-4629.

262 Guilyardi, E. (2006), El Niño-mean state-seasonal cycle interactions in a multi-model
263 ensemble. *Clim. Dyn.*, **26**, 329-348.

264 Guilyardi, E., and Coauthors (2009a), Understanding El Niño in ocean-atmosphere general
265 circulation models: Progress and challenges. *Bull. Amer. Meteor. Soc.*, **90**, 325-240.

266 Guilyardi, E., and Coauthors (2009b), Atmospheric feedbacks during ENSO in a coupled
267 GCM with a modified atmospheric convection scheme. *J. Climate*, **22**, 5698-5718.

268 Guilyardi, E., and Coauthors (2012), A first look at ENSO in CMIP5. *CLIVAR exchanges*, 17,

269 29-32.

270 Kang, I.-S., and J.-S. Kug (2002), El Niño and La Niña sea surface temperature anomalies:
 271 Asymmetry characteristics associated with their wind stress anomalies. *Geophys. Res.*
 272 *Lett.*, **107**, doi:10.1029/2001JD000393.

273 Kang, I.-S., E. K. Jin, and K.-H. An (2006), Secular increase of seasonal predictability for the
 274 20th century. *Geophys. Res. Lett.*, **33**, L02703.

275 Kaplan, A., and Coauthors (1998), Analyses of global sea surface temperature 1856-1991. *J.*
 276 *Geophys. Res.*, **103**, 18567-18589.

277 Kim, D., and Coauthors (2011), ENSO sensitivity to cumulus entrainment in a coupled GCM.
 278 *J. Geophys. Res.*, **116**, doi:10.1029/2011JD016526.

279 Kug, J.-S., and Coauthors (2008), State-dependent atmospheric noise associated with ENSO.
 280 *Geophys. Res. Lett.*, **35**, L05701.

281 Meehl, G. A., and Coauthors (2007a), Global climate projections. In *Climate Change 2007:*
 282 *The Physical Science Basis*, Solomon S *et al.* eds., Cambridge Univ. Press.

283 Meehl, G. A., and Coauthors (2007b), The WCRP CMIP3 multimodel dataset: A new era in
 284 climate change research. *Bull. Amer. Meteor. Soc.*, **88**, 1383-1394.

285 Neale, R. B., J. H. Richter, and M. Jochum (2008), The impact of convection on ENSO: From
 286 a delayed oscillator to a series of events. *J. Climate*, **21**, 5904-5924.

287 Park, W., and Coauthors (2009), Tropical Pacific climate and its response to global warming
 288 in the Kiel climate model. *J. Climate*, **22**, 71-92.

289 Philip, S. Y., M. Collins, G. J. van Oldenborgh, B. J. J. M. van den Hurk (2010), The role of
 290 atmosphere and ocean physical processes in ENSO in a perturbed physics coupled
 291 climate model. *Ocean Sci.*, **6**, 441-459.

292 Rayner, N. A., and Coauthors (2003), Global analyses of sea surface temperature, sea ice, and
 293 night marine air temperature since the late nineteenth century. *J. Geophys. Res.*, **108**, doi:
 294 10.1029/2002JD 002670.

295 Taylor, K. E., R. J. Stouffer, and G. A. Meehl (2012), An overview of CMIP5 and the
 296 experiment design. *Bull. Amer. Meteorol. Soc.*, **90**, 485-498.

297 Toniazzo, T., M. Collins, and J. Brown (2008), The variation of ENSO characteristics

298 associated with atmospheric parameter perturbations in a coupled model. *Clim. Dyn.*, **30**,
299 643-656.

300 van Oldenborgh, G. J., S. Philip, and M. Collins (2005), El Niño in a changing climate: a
301 multi-model study. *Ocean Sci.*, **2**, 267-298.

302 Vecchi G. A., and Coauthors (2006), Weakening of tropical Pacific atmospheric circulation
303 due to anthropogenic forcing. *Nature*, **441**, 73-76.

304 Vecchi, G. A., and A. T. Wittenberg (2010): El Niño and our future climate: Where do
305 we stand? Wiley Interdisciplinary Reviews: *Climate Change*, **1**, 260-270.
306 doi:10.1002/wcc.33

307 Watanabe, M., M. Chikira, Y. Imada, and M. Kimoto (2011), Convective control of ENSO
308 simulated in MIROC5. *J. Climate*, **24**, 543-562.

309 Watanabe, M., and A. T. Wittenberg (2012), A method for disentangling El Niño-mean state
310 interaction. *Geophys. Res. Lett.*, **39**, doi:10.1029/2012GL052013.

311 Wittenberg, A. T. (2009), Are historical records sufficient to constrain ENSO simulations?
312 *Geophys. Res. Lett.*, **36**, L12702.

313 Xie, P., and P. A. Arkin (1997), Global precipitation: A 17-year monthly analysis based on
314 gauge observations, satellite estimates, and numerical model outputs. *Bull. Amer. Meteor.*
315 *Soc.*, **78**, 2539-2558.

316 Yeh, S.-W., Y. G. Park, and B. P. Kirtman (2006), ENSO amplitude changes in climate
317 change commitment to atmospheric CO₂ doubling. *Geophys. Res. Lett.*, **33**, L13711.

318

319 **Figure captions**

320 **Figure 1** Relationship between ENSO amplitude and mean state in combined parameter
321 ensemble. (a) Correlation of the annual-mean precipitation climatology with the std dev of the
322 Niño 3 SST anomalies ($\sigma_{\text{niño}}$) in the control experiments, imposed on the ensemble-mean
323 precipitation climatology (contour, interval of 2.5 mm dy⁻¹). The 95% statistical significance
324 is denoted by dots. (b)-(e) Scatter diagram of $\sigma_{\text{niño}}$ against the climatological precipitation

325 over the Niño 3 region ($\bar{P}_{\text{niño}}$) in each of the parameter ensembles. The ‘×’ mark indicates the
326 observational estimate for the late 20th century [Xie and Arkin 1997, Rayner et al. 2003]. The
327 blue and red symbols represent the values in the control and increased CO₂ experiments,
328 respectively. The regression slope and the ensemble average are indicated by straight line and
329 a filled symbol for each set of the experiments.

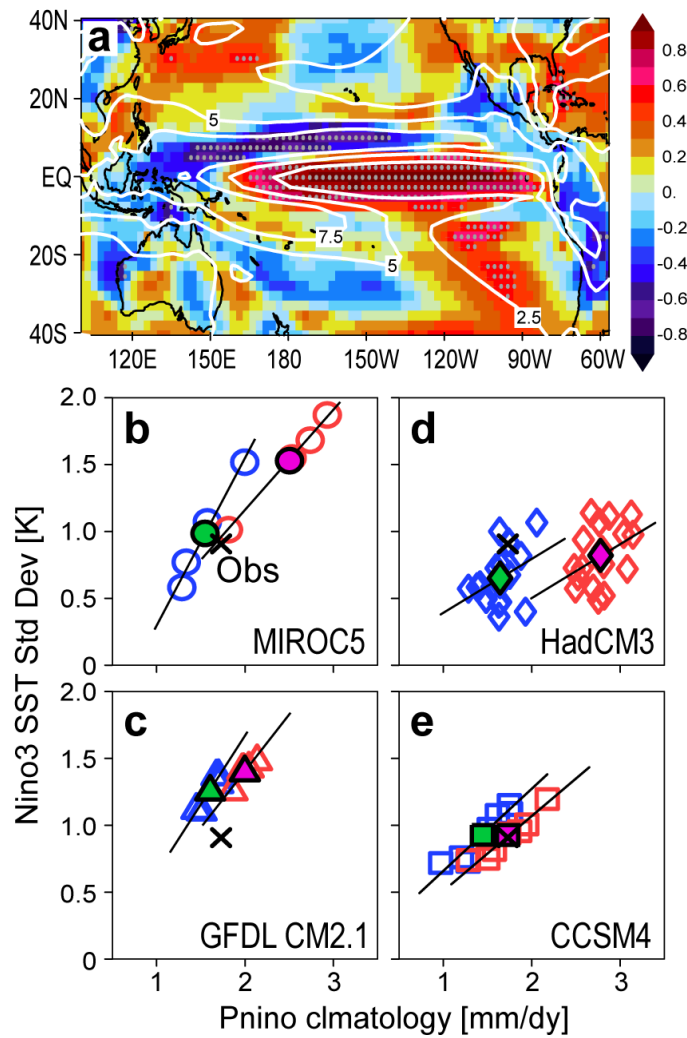
330 **Figure 2** Reconstruction of $\bar{P}_{\text{niño}}$ in the combined PPEs, following Eq. (1)-(2). The full
331 reconstruction and partial contributions to the diversity in $\bar{P}_{\text{niño}}$ by each of the four terms in
332 Eq. (2), i.e., changes in the precipitation sensitivity and mean SST, ENSO amplitude feedback,
333 and nonlinearity [cf. Watanabe and Wittenberg 2012], are shown for each parameter ensemble.
334 The diversity in $\bar{P}_{\text{niño}}$ and its reconstruction is presented by the std dev in the ensembles
335 (black vertical lines). Inset panel shows an example of the PDF for the Niño 3 SST (black)
336 and the precipitation composite sorted by the PDF (blue with shading for the error range)
337 calculated with HadCM3 data.

338 **Figure 3** Relationship between ENSO amplitude and mean precipitation in multi-model
339 ensembles, represented as the scatter diagram of $\sigma_{\text{niño}}$ against $\bar{P}_{\text{niño}}$. (a) Estimates for
340 1940–1999 in the CMIP3 and CMIP5 models (blue and red symbols, respectively), with the
341 ensemble means and the regression slopes indicated by the dashed and solid lines, and (b)
342 each of the ensemble historical experiments for 1940-1999 in CMIP5 (only for models with
343 more than three members). The respective regression slopes and the observational estimate
344 are indicated as in Fig. 1b-e.

345 **Figure 4** The $\sigma_{\text{niño}} - \bar{P}_{\text{niño}}$ relationship between different eras of the CMIP5 MME. (a) The
346 change in $\sigma_{\text{niño}}$ and $\bar{P}_{\text{niño}}$ from the pre-industrial (1850 condition) to 1940-1999 periods,

347 and (b) the change from 1940-1999 to 2040-2099 periods, the latter derived from the RCP4.5
 348 experiments. The MME averages are indicated by blue circles. The regression line and the
 349 correlation coefficients are also shown. The dashed lines in (a) indicate differences in $\sigma_{\text{niño}}$
 350 between 1871-1930 and 1940-1999 estimated from two observational SST data sets [Rayner
 351 *et al.* 2003, Kaplan *et al.* 1998].

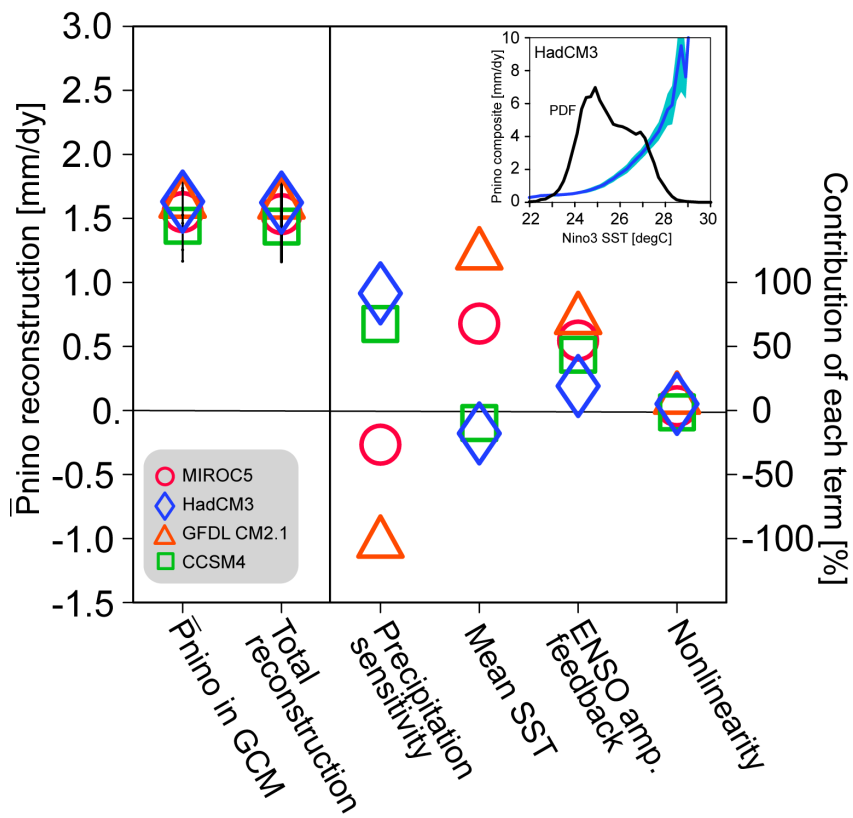
352



353

354 **Figure 1.**

355



356

357 **Figure 2.**

358

359

360

361

362

363

364

365

366

367

368
369
370
371
372
373
374
375
376
377
378
379
380
381
382
383
384
385
386

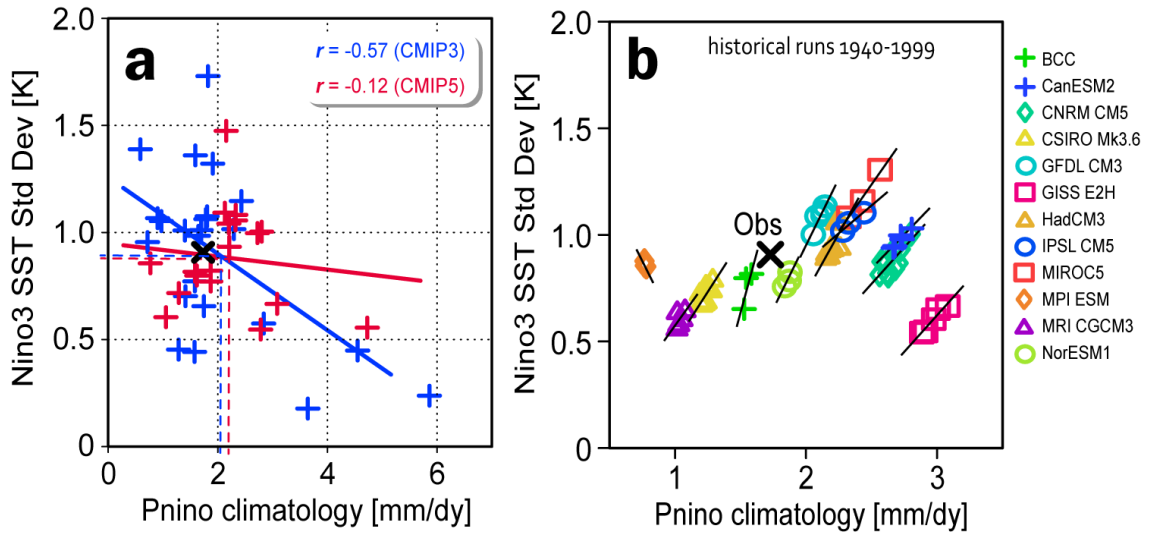
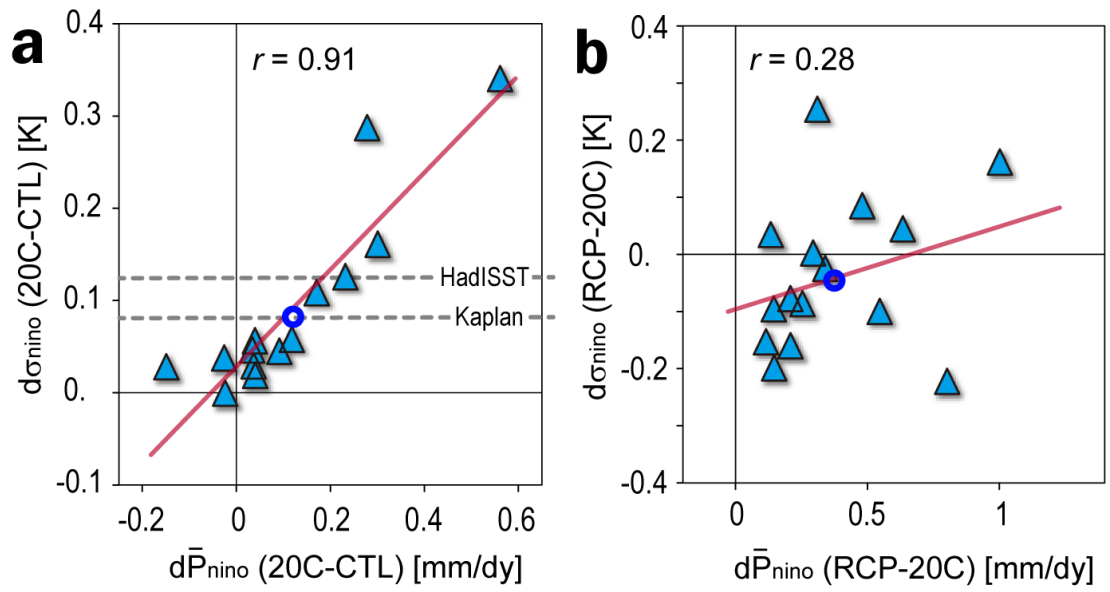


Figure 3.



387

388 **Figure 4.**

389

390

391